Rigid Amorphous Phase and Low Temperature Melting Endotherm of Poly(ethylene terephthalate) Studied by Modulated Differential Scanning Calorimetry

M. SONG*

IPTME, Loughborough University, Loughborough LE11 3TU, United Kingdom

Received 10 May 2000; accepted 2 December 2000

ABSTRACT: The rigid amorphous phase, the low temperature melting endotherm, and their development with thermal treatment in poly(ethylene terephthalate) (PET) were investigated by means of modulated differential scanning calorimetry. The differential of the reversing heat capacity and nonreversing heat flow signals were used to analyze the behavior of the glass transition and the low temperature melting endotherm. With increasing annealing time, the increment of the heat capacity at the glass-transition temperature decreased and the increment of heat capacity at the annealing temperature increased. It was suggested that the origin of the low temperature melting endotherm mainly resulted from the transition of the rigid amorphous fraction for the PET used. The glasslike transition of the rigid amorphous fraction occurred between the glass transition and melting. © 2001 John Wiley & Sons, Inc. J Appl Polym Sci 81: 2779–2785, 2001

Key words: modulated differential scanning calorimetry; crystallization; poly(ethylene terephthalate)

INTRODUCTION

The differential scanning calorimetry (DSC) thermograms of poly(ether ether ketone),[1] poly(ethylene terephthalate) (PET),[2] and poly(phenylene sulfide)[3] show two melting endotherms after isothermal crystallization or annealing. The low temperature melting endotherm increases in magnitude and shifts to higher temperature with increasing crystallization or annealing temperatures or time.

Cheng et al.[2] stated that the endotherm is the result of an annealing process. Lee and Porter[1] indicated that this phenomenon results from a melting–recrystallization process. Velikov and Marand[4] demonstrated that the kinetics of the development of the low temperature melting endotherms resembles the kinetics of an enthalpy relaxation process. They suggested that the origin of the low temperature melting endotherm lies in the enthalpy recovery of a rigid amorphous fraction. Lu and Cebe[3] also indicated that the low temperature melting endotherm results from the transition associated with the rigid amorphous fraction. Bassett et al.[5] suggested that the double endothermic behavior is associated with the melting of a bimodal distribution of crystalline lamellar thicknesses.

Several studies[6–10] used real-time small angle X-ray scattering (SAXS) measurements to indicate that the low temperature melting endotherm is caused by the melting of thinner lamellae inserted between layers of thicker ones and the higher temperature endotherm is caused by melt-

*E-mail: m.song@lboro.ac.uk.

Journal of Applied Polymer Science, Vol. 81, 2779–2785 (2001)

ing of the remaining thicker lamellae. This model is referred to as the lamellar insertion model, which is an extension of the dual population model.[5]

Kruger and Zachmann[10] concluded that the low temperature melting endotherm is caused by partial melting within a lamellar stack rather than the melting of complete lamellar stacks. More recent work by Verma et al.[11] estimated the lamellar and amorphous layer thickness to test for the Kruger–Zachmann conclusion. Verma et al.[11] indicated that the melting–recrystallization model and the lamellar insertion model are ruled out as possible explanations for the origin of the low temperature melting endotherm in semicrystalline polymers because it was observed from the SAXS data that the average amorphous layer thickness did not decrease during the development of the low temperature endotherm but did decrease during melting at the temperature corresponding to the low temperature endotherm. They suggested that the origins of the low and high temperature melting endotherms lie in the melting of secondary and primary lamellar stacks, respectively. The secondary lamellar stacks consist of thinner lamellae and thicker amorphous layers as compared to the primary lamellae, which results in the high temperature endotherm.

Lattimer et al.[12] used transmission electron microscopy to observe melting of thinner lamellae at temperatures corresponding to the lower temperature melting endotherm. Although the works of Lovinger and Davis[13] and Marand and Prasad[14] suggest that the actual morphology consists of stacks of crystalline lamellae separated by amorphous regions of significant dimensions, a detailed morphological picture of semicrystalline materials has not emerged,[11] especially for providing an understanding of the origin of the low temperature melting endotherm and the rigid amorphous fraction.

The following two topics are addressed in this study: the origin of the low temperature melting endotherm and the rigid amorphous fraction. To these ends, modulated DSC (MDSC) measurements were performed on PET.

EXPERIMENTAL

Sample Preparation

The PET samples used in this study were obtained from Aldrich. All samples were first dried in a vacuum at 120°C for 30 h. The number- and weight-average molecular weights were 12,600 and 24,700, respectively. These values were determined by GPC calibrated with polystyrene standards.

The PET1 sample, which was in the form of a 0.3 mm thick film, was made by compression molding at 300°C for 10 min and then put into liquid nitrogen together with the mold. The increment of the heat capacity (ΔC_p) of PET1 at the glass-transition temperature (T_g) was found to be 0.28 J g^{-1} $°C^{-1}$. The measurement method and reproducibility for ΔC_p at the T_g can be found in Hourston et al.[15] The value for a fully amorphous PET is reported[16] to be 0.35 J g^{-1} $°C^{-1}$. It is believed that the PET1 is not fully amorpous.

The PET1 was isothermally cold crystallized (at 110°C) within the sample cell of the DSC calorimeter.

The PET melt crystallization (PET2) was conducted in the DSC cell by cooling at a rate of 10°C/min from the melt (300°C for 10 min) to 40°C. Then the PET2 was annealed at 155°C for different times.

The PET3 sample was obtained by heating a PET sample at 300°C for 10 min and then quenching to −20°C at 60°C/min. The ΔC_p was 0.34 J g^{-1} $°C^{-1}$.

Thermal analysis was subsequently performed using model 2920 MDSC equipment from TA Instruments. The temperature and baseline were calibrated as for conventional DSC. A scan rate of 3°C/min was used with a temperature modulation period of 60 s and a temperature modulation amplitude of 0.5°C. An average sample weight of 8 mg was used to maximize the signal and reduce the heat transfer delay. Nitrogen was used as the heat transfer gas at a flow rate of 35 mL/min.

RESULTS AND DISCUSSION

The MDSC scans are shown in Figure 1 for PET2 annealed for different times at 155°C. Two melting endotherm peaks for the annealed samples are clearly seen. As the annealing time was increased, the low temperature melting endotherm shifted to higher temperatures. The high temperature melting endotherm did not change in position. The isothermally cold crystallized samples (PET1) also showed the same behavior. The peak temperatures and heats of fusion are listed in Table I. Note that the low temperature melting

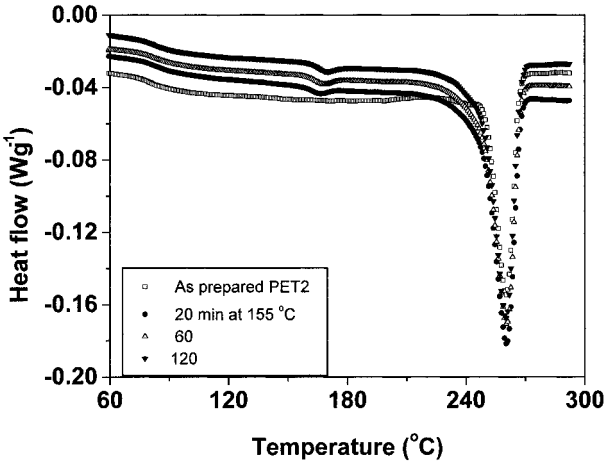

Figure 1 The heat flow versus temperature for PET2 specimens annealed at 155°C for different times.

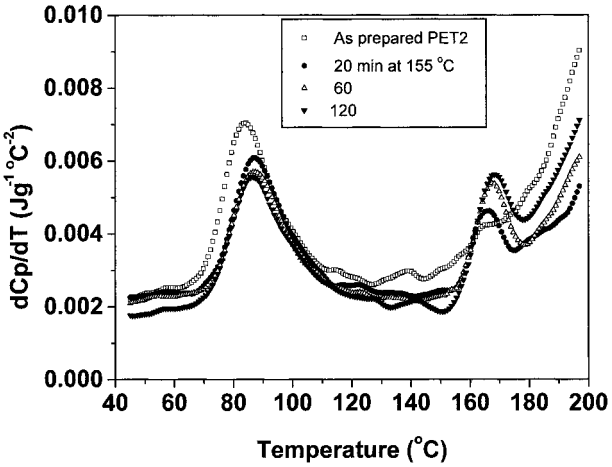

Figure 2 The differential of the reversing heat capacity (dC_p/dT) versus the temperature for PET2 specimens annealed at 155°C for different times.

endotherm is dependent on the annealing temperature.

Figures 2 and 3 show the differential of the heat capacity (dC_p/dT) versus the temperature for PET2 for different annealing times at 155°C and for PET1 at different cold crystallization times at 110°C, respectively.

The ΔC_p values at the T_g decreased and increased at the annealing temperature (T_a) with the annealing time. The results are shown in Figure 4 for PET1 and in Figure 5 for PET2. A part of the amorphous phase formed a new fraction, which showed a transition at the annealing temperature. With increasing annealing time the sum of the ΔC_p at the T_g and the T_a became independent of the time. No change in the crystal fraction was observed after the treatment for PET2 after 20 min and for PET1 after 60 min.

Figure 6 shows the calculation of the ΔC_p value for the new fraction. The ΔC_p value is equal to the area of ABCA.

Figures 7 and 8 show the change of the nonreversing heat flow with temperature at different times for PET2 annealed at 155°C and PET1 annealed at 110°C, respectively. The low temperature melting endotherm peak area increased with the annealing time.

Figure 9 is a comparison of the low temperature endotherm and enthalpy relaxation at the T_g in PET1. The PET1 was annealed at 150°C for 60 min and then annealed at 65°C for 600 min.

A comparison of Figures 7, 8, and 9 seemed to show that the low temperature melting endotherm was related to enthalpy relaxation. The nonreversing heat flow signal with the annealing time was similar to that for physical aging of glassy polymers.[17] Also, the decrease of the weight fraction of the amorphous phase at the T_g was approximately equal to the increase of the weight fraction of the annealing temperature dependent fraction (new fraction). If the low tem-

Table I Melting Temperatures and ΔH Values for PET1 and PET2 at Different Annealing Times

Sample	Annealing Time (min)	T_m (°C)	ΔH (Jg^{-1})	T^a (°C)	ΔH^a (Jg^{-1})
PET1	60	256	39.3	118	2.1
	180	256	40.2	120	3.4
	2700	256	39.5	127	4.8
PET2	20	261	40.7	166	0.75
	60	261	40.0	168	0.84
	120	260	39.6	170	1.0

[a] Low melting.

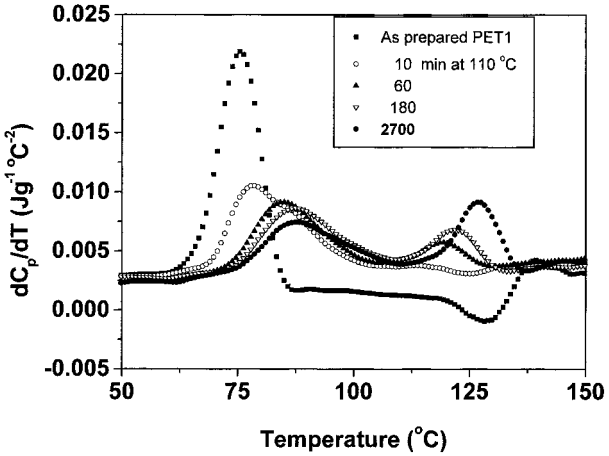

Figure 3 The differential of the reversing heat capacity (dC_p/dT) versus the temperature for PET1 specimens annealed at 110°C for different times.

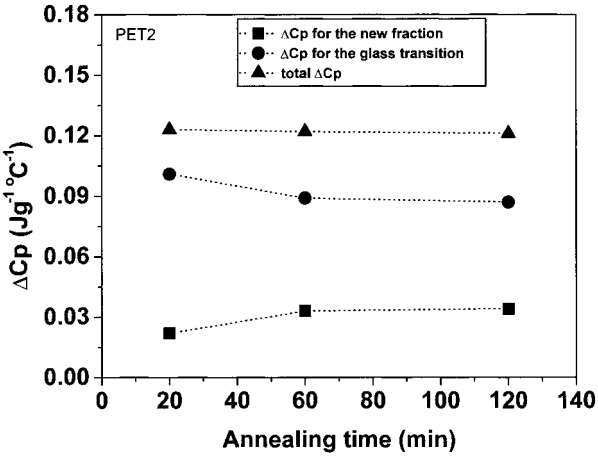

Figure 5 The increment of the heat capacity (ΔC_p) of PET1 versus the annealing time for the amorphous phase and for the new fraction.

perature endotherm resulted from enthalpy relaxation, the relaxation enthalpy (ΔH) would have a nonlinear relationship with the content of the new fraction. Figure 10 shows the change of ΔH with ΔC_p for the new fraction. The relationship between ΔH and ΔC_p was clearly linear. Another experiment was designed to confirm this. First, the PET2 was annealed at 170°C for 15 min (sample D). Second, another PET2 sample was annealed at 170°C for 15 min and then annealed at 152°C for 40 min (sample C). Figure 11 shows the results for samples C and D. The peak area from the nonreversing heat flow signal was 0.72 J g^{-1} for C and 0.70 J g^{-1} for D. Thus, no peak area change was found. Perhaps the enthalpy relaxation of the new fraction contributed so little that it could not be measured. However, we believe that the low temperature melting endotherm cannot be described solely by the enthalpy relaxation model.

The lamellar insertion model proposes that the low melting endotherm is caused by melting of thinner lamellae inserted between thicker ones. This implies that the long period, the average lamellar thickness, and the amorphous layer thickness would increase upon heating through the low temperature melting endotherm. However, Verma et al.[11] demonstrated that, although the long period and the lamellar thickness do rise during melting, the amorphous layer thickness

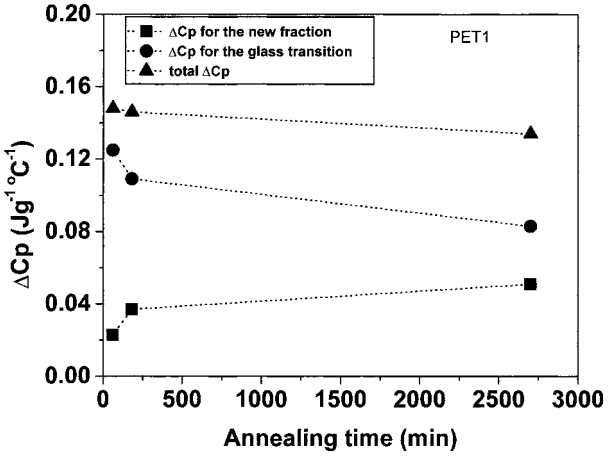

Figure 4 The increment of the heat capacity (ΔC_p) of PET1 versus the annealing time for the amorphous phase and for the new fraction.

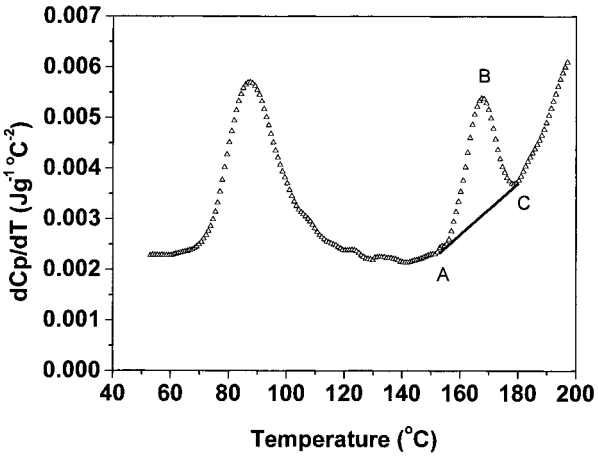

Figure 6 The calculation of the increment of the heat capacity (ΔC_p) value for the new fraction, where ΔC_p = ABCA area.

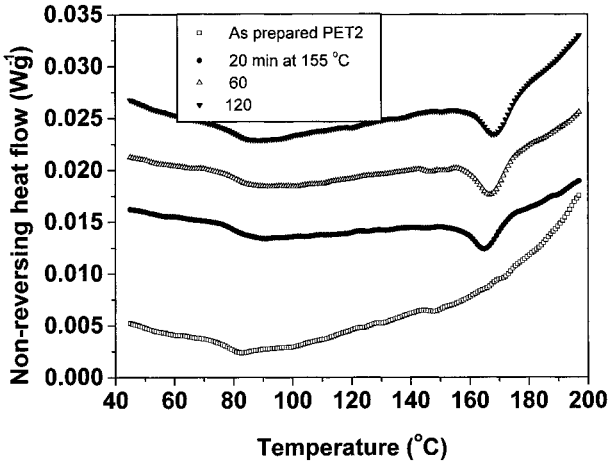

Figure 7 The nonreversing heat flow versus the temperature for PET2 specimens annealed at 155°C for different times.

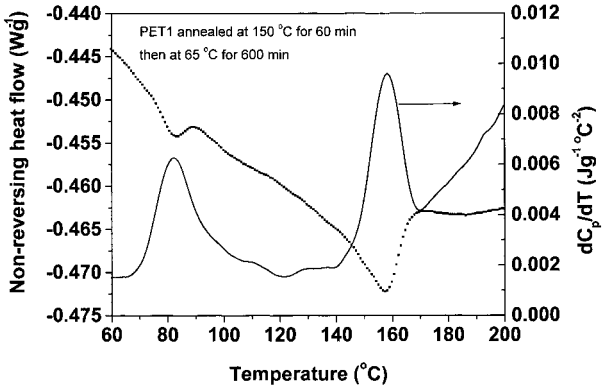

Figure 9 The differential of the reversing heat capacity (dC_p/dT) and nonreversing heat flow versus the temperature for a PET1 specimen annealed at 150°C for 60 min and then at 65°C for 600 min.

decreases. The PET2 was annealed at 155°C for 20 min and heated momentarily to 180°C, then immediately quenched to liquid nitrogen temperature (sample E). The ΔC_p value was 0.130 for sample E and 0.107 J g^{-1} $°C^{-1}$ for sample B, which was annealed at 155°C for 20 min. The weight fraction of the amorphous phase in E increased. The ΔC_p of E was the same as that of the as prepared PET2. The MDSC results indicated that the low endotherm may have been the result of an annealing process. With increasing annealing time the low temperature melting endotherm increased in magnitude and the amount of the amorphous phase at the T_g decreased. It is very difficult to imagine that the new fraction formed from the amorphous phase crystallized completely.

Recent studies[2,16,18–21] indicated that the amorphous phase in these semicrystalline polymers is complex. Suzuki et al.[16] proposed the idea of a "rigid amorphous fraction." The rigid amorphous fraction is that portion of the amorphous phase that does not undergo a distinct glass-transition relaxation. Only the most mobile, or liquid-like, amorphous phase undergoes the glass-transition relaxation process during DSC testing. This fraction has very limited mobility. It follows from this that the rigid amorphous fraction does not contribute to either the glass transition or the heat of melting of the crystalline part.[22]

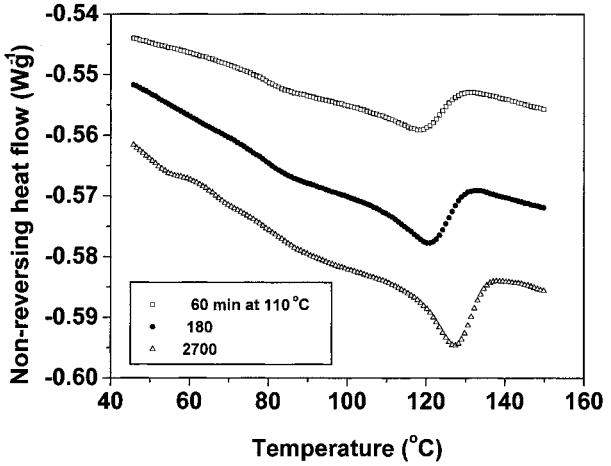

Figure 8 The nonreversing heat flow versus the temperature for PET1 specimens annealed at 110°C for different times.

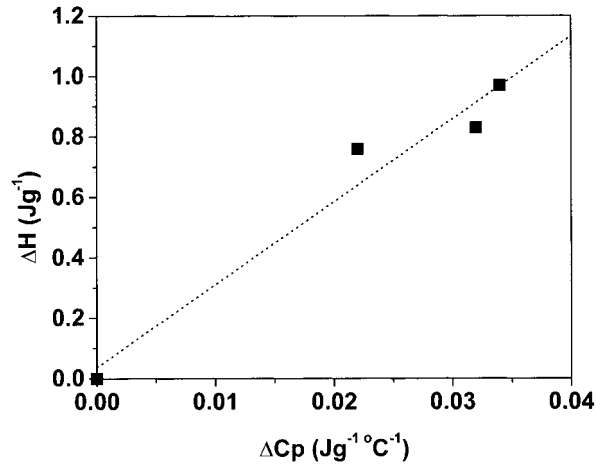

Figure 10 The peak area (relaxation enthalpy, ΔH) of the new fraction versus its increment of the heat capacity (ΔC_p).

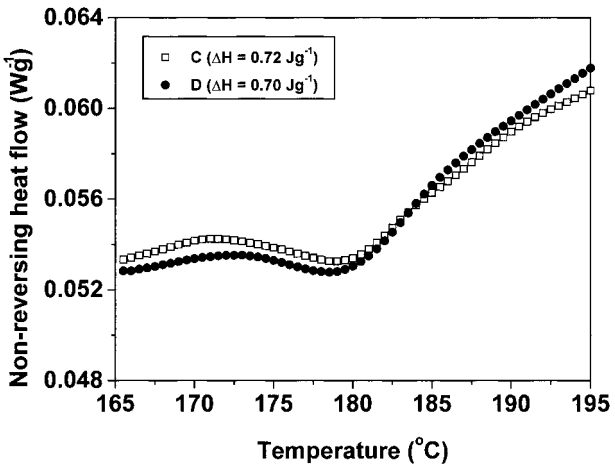

Figure 11 The nonreversing heat flow for samples C and D.

The MDSC experimental results in Figure 12 (PET3) give a comparison of the dC_p/dT versus the temperature signal for the amorphous PET and PET2. The value of the dC_p/dT for PET2 was found to be larger than that for the amorphous PET between 100 and 135°C. This showed that there was some kind of transition.

The rigid amorphous fraction may be the crystal–amorphous interphase in which some segments are located in the crystal phase and some segments lie in the amorphous phase. Because of the crystal phase, the rigid amorphous fraction has limited mobility. Consider the results shown in Figure 12 again. The plot is redrawn with a different scale in Figure 13. The dC_p/dT versus

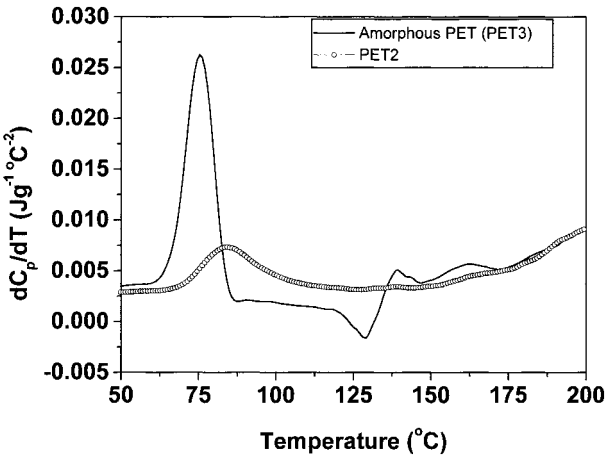

Figure 12 The differential of the reversing heat capacity (dC_p/dT) versus the temperature signals for amorphous PET (PET3) and PET2.

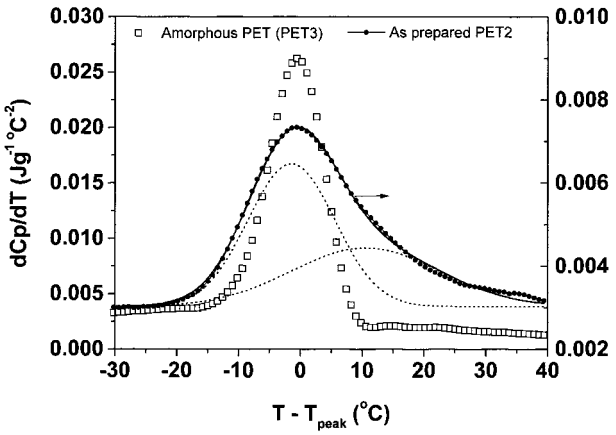

Figure 13 A comparison of the differential of the reversing heat capacity (dC_p/dT) versus the temperature signal for amorphous PET (PET3) and for PET2. The dots are the peak resolution results that can be described by a Gaussian function of the heat capacity, the glass-transition temperature, and the half-width of the peak.[23]

temperature signal for PET2 is much broader. By comparing the dC_p/dT signal of amorphous PET (PET3) using the peak resolution[23] we can separate the broad dC_p/dT signal into two single transition peaks. The transition peak that has a higher peak temperature value may result from the rigid amorphous fraction. With thermal treatment above the T_g, more rigid amorphous fraction is created. During the annealing process the part of the amorphous phase near to the crystal phase may become highly ordered. Thus, it was concluded that the glasslike transition of the rigid amorphous fraction occurred between the glass transition and melting.

CONCLUSIONS

The dC_p/dT and nonreversing heat flow signals can used to analyze the behavior of the glass transition and the low temperature melting endotherm. Increasing annealing time causes the ΔC_p at the T_g to decrease and the ΔC_p at the T_a to increase. The origin of the low temperature melting endotherm mainly results from the transition of the rigid amorphous fraction. The glasslike transition of the rigid amorphous fraction occurs between the glass transition and melting.

REFERENCES

1. Lee, Y.; Porter, R. S. Macromolecules 1987, 20, 1336.

2. Cheng, S. Z. D.; Cao, M. Y.; Wunderlich, B. Macromolecules 1986, 19, 1868.
3. Lu, X. X.; Cebe, P. Polymer 1996, 37, 4857.
4. Velikov, V.; Marand, H. Macromolecules (preprint).
5. Bassett, D. C.; Olley, R. H.; Raheil, I. A. M. Polymer 1988, 29, 1745.
6. Haiso, B. S.; Gardner, K. H.; Wu, D. Q.; Liang, B.; Chu, B. ACS Polym Prepr 1992, 33, 265.
7. Haiso, B. S.; Gardner, K. H.; Wu, D. Q.; Chu, B. Polymer 1993, 34, 3986.
8. Haiso, B. S.; Gardner, K. H.; Wu, D. Q.; Chu, B. Polymer 1993, 34, 3996.
9. Wang, J.; Alvarez, M.; Zhang, W.; Wu, Z.; Li, Y.; Chu, B. Macromolecules 1992, 25, 6943.
10. Kruger, K. N.; Zachmann, H. G. Macromolecules 1993, 26, 5202.
11. Verma, R. K.; Velikov, V.; Kander, R. G.; Marand, H.; Chu, B.; Haiso, B. Polymer 1996, 37, 5357.
12. Lattimer, M. P.; Hobbs, J. K.; Hill, M. J.; Barham, P. J. Polymer 1992, 33, 3971.
13. Lovinger, A. J.; Davis, D. D. Macromolecules 1986, 19, 1861.
14. Marand, H.; Prasad, A. Macromolecules 1992, 25, 1731.
15. Hourston, D. J.; Song, M.; Pollock, H. M.; Hammiche, A.; Reading, M. J Therm Ann 1997, 49, 209.
16. Suzuki, H.; Grebowicz, J.; Wunderlich, B. Makromol Chem 1984, 186, 1109.
17. Hourston, D. J.; Song, M.; Pollock, H. M.; Hammiche, A.; Reading, M. Polymer, 1996, 37, 371.
18. Lau, S. F.; Wunderlich, B. J Polym Sci Polym Phys 1984, 22, 379.
19. Grebowiz, J.; Lau, S. F.; Wunderlich, B. J Polym Sci Polym Symp 1984, 71, 19.
20. Huo, P. P.; Cebe, P. Macromolecules 1992, 25, 902.
21. Cebe, P.; Huo, P. P. Thermochim Acta 1994, 238, 229.
22. Hohne, G. W.; Hemminger, W.; Flammersheim, H. J. Differential Scanning Calorimetry: An Introduction for Practitioners; Springer–Verlag: Berlin, 1996; p 117.
23. Song, M.; Hourston, D. J.; Schafer, F.; Pollock, H. M.; Hammiche, A. Thermochim Acta 1997, 304/305, 335.